Mon. Not. R. Astron. Soc. **000**, 000–000 (0000) Printed 20 November 2015 (MN LATEX style file v2.2)

Supermassive star formation via episodic accretion: protostellar disc instability and radiative feedback efficiency

Y. Sakurai[1], E. I. Vorobyov[2,3], T. Hosokawa[1,4], N. Yoshida[1,5], K. Omukai[6] and H. W. Yorke[7]

[1] *Department of Physics, School of Science, University of Tokyo, Bunkyo, Tokyo 113-0033, Japan*
[2] *Department of Astrophysics, The University of Vienna, Vienna, 1180, Austria*
[3] *Research Institute of Physics, Southern Federal University, Rostov-on-Don 344090, Russia*
[4] *Research Center for the Early Universe, University of Tokyo, Bunkyo, Tokyo 113-0033, Japan*
[5] *Kavli Institute for the Physics and Mathematics of the Universe (WPI), Todai Institutes for Advanced Study, the University of Tokyo, Kashiwa, Chiba 277-8583, Japan*
[6] *Astronomical Institute, Tohoku University, Sendai, Miyagi 980-8578, Japan*
[7] *Jet Propulsion Laboratory, California Institute of Technology, Pasadena, CA 91109, USA*

©2015. All rights reserved.

arXiv:1511.06080v1 [astro-ph.SR] 19 Nov 2015

Draft version 20 November 2015

ABSTRACT

The formation of supermassive stars (SMSs) is a potential pathway to seed supermassive black holes in the early universe. A critical issue for forming SMSs is stellar UV feedback, which may limit the stellar mass growth via accretion. In this paper we study the evolution of an accreting SMS and its UV emissivity under conditions of realistic variable accretion from a self-gravitating circumstellar disc. First we conduct a 2D hydrodynamical simulation to follow the long-term protostellar accretion until the stellar mass exceeds 10^4 $M_\odot$. The disc fragments due to gravitational instability, creating a number of small clumps that rapidly migrate inward to fall onto the star. The resulting accretion history is thus highly time-dependent: short episodic accretion bursts are followed by longer, relative quiescent phases. We show that the circumstellar disc for the so-called direct collapse model is more unstable and generates greater variability over shorter timescales than normal Pop III cases. We conduct a post-process stellar evolution calculation using the obtained accretion history. Our results show that, regardless of the strong variability of the accretion rates, the stellar radius monotonically increases with almost constant effective temperature at $T_{\rm eff} \simeq 5000$ K as the stellar mass increases. The resulting UV feedback is too weak to hinder mass accretion due to the low flux of stellar UV photons, thus verifying our implicit assumption of no stellar feedback during the hydrodynamic simulations. The insensitivity of stellar evolution to variable accretion is attributed to the fact that typical timescales of variability, $\lesssim 10^3$ years, are too short to affect the stellar structure. We argue that this evolution will continue until the SMS eventually collapses to produce a massive black hole by the general relativistic instability after the stellar mass reaches $\gtrsim 10^5$ $M_\odot$.

Key words: stars: formation - galaxies: formation - cosmology: theory - early Universe

1 INTRODUCTION

Supermassive black holes (SMBHs) with $\gtrsim 10^9$ $M_\odot$ already exist as early as at $z \gtrsim 6$ (e.g., Fan et al. 2003, 2006; Willot & Christmann 2010; Mortlock et al. 2011; Wu et al. 2015). Formation of such SMBHs is a subject of intense study, since little is known about the processes leading to the accumulation of such a tremendous amount of mass within a billion years.

A possible scenario for the early formation of SMBHs is the so-called direct collapse model: A massive seed BH with $\sim 10^5$ $M_\odot$ increases its mass through accretion and mergers to become a SMBH (e.g., Bromm & Loeb 2003). The massive seed BH can be formed by the collapse of a super-

massive star (SMS) with $\sim 10^5\ M_\odot$. The SMS is supposed to form under special conditions which allow very rapid protostellar accretion at an average rate of $\dot{M}_* \gtrsim 0.1\ M_\odot\ \mathrm{yr}^{-1}$. The proposed possible conditions include, e.g., gas clouds irradiated by strong photodissociating background (e.g., Sugimura, Omukai & Inoue 2014; Agarwal et al. 2015; Latif & Volonteri 2015), and dense shocked gas created through the formation of protogalaxies (e.g., Inayoshi & Omukai 2012; Fernandez et al. 2014; Inayoshi, Visbal & Kashiyama 2015).

A potential obstacle for the formation of SMSs is UV feedback from the protostar itself, which might halt stellar mass growth via accretion (e.g., McKee & Tan 2008; Hosokawa et al. 2011). For normal Pop III cases with $\dot{M}_* \lesssim 0.04\ M_\odot\ \mathrm{yr}^{-1}$, the protostar enters the so-called Kelvin-Helmholtz (KH) contraction stage at some point. The stellar effective temperature rises as the star contracts, so that UV feedback operates with a copious flux of UV photons. However, recent studies predict a qualitatively different evolution at higher accretion rates $\gtrsim 0.04\ M_\odot\ \mathrm{yr}^{-1}$, i.e., for the direct collapse case (e.g., Hosokawa et al. 2013; Schleicher et al. 2013); the protostar monotonically inflates with increasing stellar mass and remains at a low effective temperature $T_{\rm eff} \simeq 5000$ K (named as the "supergiant protostar" stage). At this low effective temperature, very few ionizing photons are emitted by the star.

The above cited work assumed constant accretion rates for simplicity. In reality, however, mass accretion occurring through self-gravitating circumstellar discs should be highly time variable. Such a disc often fragments to form clumps, some of which could be ejected, but most of which migrate inward through the disc. Accretion rates are greatly enhanced for a short time when the clump falls onto the star. The burst event is normally followed by a quiescent phase, where accretion almost ceases for a while. Numerical simulations predict that such episodic accretion commonly appears both in present-day and primordial star formation (e.g., Vorobyov & Basu 2006, 2015; Machida, Inutsuka & Matsumoto 2010; Smith et al. 2012; Greif et al. 2012; Vorobyov, DeSouza & Basu 2013; Hosokawa et al. 2015). Although still limited, recent studies have also reported signatures of disc fragmentation for the direct collapse cases (e.g., Regan, Johansson & Haehnelt 2014; Becerra et al. 2015).

Variable accretion may allow the star to contract, as the accretion rates can temporarily fall below $\simeq 0.04\ M_\odot\ \mathrm{yr}^{-1}$, the critical value for bloating the star. Sakurai et al. (2015, hereafter SHYY15) have calculated the stellar evolution for various episodic accretion histories, assuming periodic high and low states of accretion with a fixed mean value at $0.1\ M_\odot\ \mathrm{yr}^{-1}$. They show that the star can contract if quiescent phases with $\dot{M}_* \ll 0.04\ M_\odot\ \mathrm{yr}^{-1}$ continue for $\Delta t_{\rm q} \gtrsim 10^3\ \mathrm{yr}\ [M_*/500\ M_\odot]^{1/2}$. Once the star contracts, the stellar effective temperature and UV emissivity rapidly rise. A longer quiescent phase results in a smaller radius and thus a larger flux of UV photons, which potentially allows an HII region to expand around the star.

SHYY15 modeled accretion histories with analytic functions to study how stellar evolution changes with different accretion histories in a controlled manner. In this paper, as a next step, we investigate stellar evolution with more realistic accretion histories. We first conduct a 2D hydrodynamical simulation following the protostellar accretion, using a central sink cell to monitor the accretion history onto the star. The resulting accretion history is highly time-dependent as the emerging circumstellar disc becomes highly gravitationally unstable. We then calculate stellar evolution using the obtained accretion history as a post process and demonstrated that the star remains in the bloated supergiant stage; the quiescent phases never last for $\Delta t_{\rm q} \gtrsim 10^3$ years when $M_* \gtrsim 500\ M_\odot$.

The rest of this paper is organized as follows. In Section 2, the methods of the hydrodynamical simulation and the stellar evolution calculation are briefly explained. In Section 3, the results of the both calculations are presented. In Section 4, we discuss the implications of these results and summarize our conclusions.

2 THE NUMERICAL APPROACH

2.1 2D hydrodynamical simulations

Our model and method for numerically studying the gravitational collapse of primordial cores are presented in Vorobyov, DeSouza & Basu (2013). Here, we briefly review the main concepts and appropriate modifications for the formation of SMSs. We follow the evolution of gravitationally unstable massive primordial cores from the isolated pre-stellar stage into the star and disc formation stages and terminate our simulations once about 50% of the initial mass reservoir has been accreted onto the star plus disc system. Once the disc is formed, it occupies the innermost region of our numerical grid. The dynamics of both the disc and envelope are followed self-consistently on one global numerical grid, which ensures correct mass infall rates onto the star plus disc system. This is an important prerequisite for studying gravitational instability and fragmentation in young circumstellar discs at all epochs (e.g. Vorobyov & Basu 2010; Machida, Inutsuka & Matsumoto 2010; Vorobyov, DeSouza & Basu 2013).

We introduce a sink cell at the inner boundary of our computational domain with a radius of $R_{\rm sc} = 110$ AU, and allow matter to freely flow into the sink cell. The radius of the sink cell is chosen to accommodate the maximum radius of the growing star. In the early pre-stellar phase of evolution, we monitor the mass accretion rate through the sink cell and introduce a central point-mass object (representing the forming star). In the subsequent evolution, approximately 95% of the accreted material is assumed to land directly onto the star, whereas the rest is contained in the sink cell in order to keep its density equal to the mean density of the gas in the innermost 10–20 AU outside the sink cell.

We solve the usual mass and momentum transport equations written in the thin-disc approximation (see Section 3.1 for justification), using a method of finite-differences with a time-explicit, operator-split procedure similar to that described by Stone & Norman (1992) for their ZEUS-2D code. Advection is performed using the third-order piecewise parabolic scheme (Colella & Woodward 1984). The gravitational acceleration includes contributions from the central point-mass star (once formed), from material in the sink cell ($r < R_{\rm sc}$), and from the self-gravity of the circumstellar disc and envelope.

The equations of mass and momentum transport are

Table 1. Parameters of the Barotropic Relation

k	γ_i	$\rho_{\rm c,i}$ (g cm^{-3})	$n_{\rm c,i}$ (cm^{-3})
1	0.965	3.38×10^{-10}	8.92×10^{13}
2	1.002	8.037×10^{-8}	2.12×10^{16}
3	1.456	7.089×10^{-7}	1.87×10^{17}
4	1.269	3.673×10^{-4}	9.69×10^{19}
5	1.614	—	—

closed with a barotropic equation of state for the gas pressure P of the following form

$$P_k = \mathcal{K}\rho^{\gamma_k}\prod_{i=1}^{k-1}\rho_{\rm c,i}^{\gamma_i-\gamma_{i+1}},\ \text{ for }\ \rho_{{\rm c},k-1}\leqslant\rho<\rho_{{\rm c},k}\,, \quad (1)$$

where $\mathcal{K}=\mathcal{R}T/(\mu\rho^{\gamma_1-1})$, $T=8000$ K is the initial gas temperature, $\mathcal{R}$ the universal gas constant, and $\mu=2.27$ the mean molecular weight of the primordial gas. Equation (1) is a piecewise fit to the detailed thermal and chemical evolution during direct collapse calculated by Omukai, Schneider & Haiman (2008) using a one-zone model. Whereas the solid red line in Figure 1 portrays their exact solution, the red dashed line represents the piecewise approximation used here. The index k used in Table 1 distinguishes between the five individual components of the approximation. Also given in Table 1 for each component k are the values of the various associated polytrope indices γ_k and the associated mass and number volume densities, $\rho_{\rm c,k}$ and $n_{{\rm c},k}$, at which transitions between k and $k+1$ occur (depicted by red dots in Figure 1). We note that when $k=1$ the product term is unity, and the pressure reduces to $P_1=\mathcal{K}\rho^{\gamma_1}$. Moreover, $\mathcal{K}$ is approximately equal to the square of the initial sound speed $c_{\rm s}^2=\mathcal{R}T/\mu$, because $\gamma_1=0.965\approx1.0$.

In our simulations, the corresponding form of the barotropic relation used in the code is

$$\mathcal{P}_k = \mathcal{K}\Sigma^{\gamma_k}\prod_{i=1}^{k-1}\Sigma_{\rm c,i}^{\gamma_i-\gamma_{i+1}},\ \text{ for }\ \Sigma_{{\rm c},k-1}\leqslant\Sigma<\Sigma_{{\rm c},k}\,, \quad (2)$$

where $\mathcal{P}$ is the vertically integrated gas pressure; the transition surface and volume mass density are related to one another through the instantaneous local scale height Z at each point in the disc via $\Sigma_{{\rm c},i}=2Z\rho_{{\rm c},i}$. The scale height Z is calculated assuming a local hydrostatic balance in the gravitational field of both the star and the disc (Vorobyov & Basu 2009).

The initial gas surface density Σ and angular velocity Ω profiles are similar to those that were considered in the context of normal population III star formation (Vorobyov, DeSouza & Basu 2013)

$$\Sigma=\frac{r_0\Sigma_0}{\sqrt{r^2+r_0^2}}\,, \quad (3)$$

$$\Omega=2\Omega_0\left(\frac{r_0}{r}\right)^2\left[\sqrt{1+\left(\frac{r}{r_0}\right)^2}-1\right]. \quad (4)$$

The radial profile of Σ is an integrated form of a Bonnor-Ebert sphere, while that of Ω is the expected differential rotation profile to accompany Equation (3) for a core contracting from near-uniform initial conditions (Basu 1997). The parameters $\Omega_0=7.22$ km s^{-1} pc^{-1}, $\Sigma_0=7.63$ g cm^{-2}, and $r_0=0.154$ pc, are the central angular velocity, central gas surface density, and the radius of a central near-constant-density plateau, respectively. They are chosen to create a gravitationally unstable core with initial mass $M_{\rm c}=26240\ M_\odot$ and ratio of rotational to gravitational energy $\beta=1.96\times10^{-2}$. Although the initial cloud mass is somewhat lower than that assumed for the direct-collapse model, where SMSs exceeding $10^5\ M_\odot$ may finally form, this is sufficient to allow us to follow the evolution for the first $\sim10^5$ years of protostellar accretion. Below we compare the resulting evolution with that discussed in Vorobyov, DeSouza & Basu (2013), who have followed the evolution for a similar duration but for the normal Pop III case.

Numerical simulations are run on a polar coordinate (r,ϕ) grid with 512×512 spatial zones. The radial points are logarithmically spaced, allowing improved numerical resolution of the inner grid, where the disc forms and evolves. The innermost cell outside the central sink has a radius $R_{\rm sc}+1.6$ AU and the radial and azimuthal resolution are about 14 AU at a radius of 1000 AU and 70 AU at a distance of 5000 AU. This resolution is sufficient to fulfill the Truelove criterion, which states that the local Jeans length must be resolved by at least four numerical cells (Truelove et al. 1997). Indeed, the Jeans length of a thin self-gravitating disc can be written as (Vorobyov 2013)

$$R_{\rm J}=\frac{\overline{c_{\rm s}}^2}{G\overline{\Sigma}}\,. \quad (5)$$

For the mean surface density of $\overline{\Sigma}\approx500$ g cm^{-2} and mean temperature $\overline{T}\approx7500$ K, typical for our disc at $r=1000-5000$ AU (see Fig. 5), the corresponding Jeans length is $R_{\rm J}\approx550$ AU and is resolved by roughly 40 grid zones at 1000 AU and 8 grid zones at 5000 AU in each direction (r,ϕ).

2.2 Stellar evolution calculations

We use the stellar evolution code STELLAR originally developed by Yorke & Bodenheimer (2008), which has been also used in SHYY15. Since the detalied description of the code is in SHYY15, we here briefly explain the main features of the code.

The code solves the basic equations of stellar evolution, including effects of mass accretion under the assumption of spherical symmetry. Nuclear reactions are considered up to helium burning (3α and {CNO} + He). Energy transport by convection is modeled by mixing length theory.

We use a grey atmosphere boundary condition for the stellar surface layer, where the accreted gas accumulates. The gas mass $\dot{M}_*\Delta t$ is added to the outermost grid cell each time step, where $\dot{M}_*$ is the accretion rate and Δt is the stellar evolution time step. The physical quantities of the accreted gas are assumed to be the same as those in the outermost grid point. This approximates an extreme case where the accreting gas slowly approaches the star and has time to adjust thermally to the stellar surface, but is not always the case because the gas can accrete with more thermal energy.

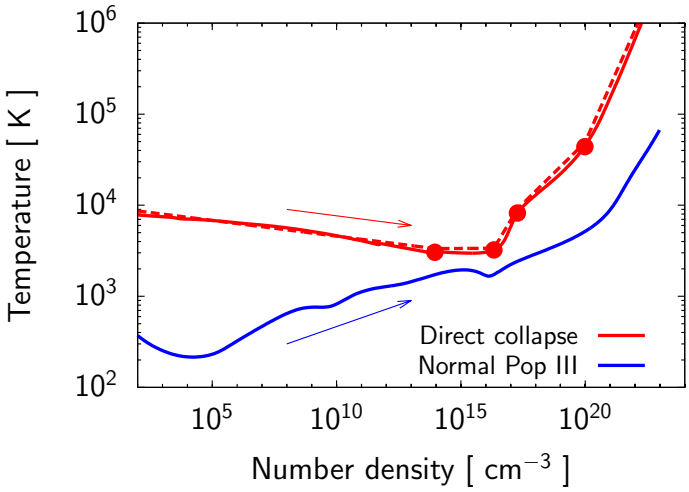

Figure 1. The temperature evolution of collapsing primordial gas as a function of the number density of hydrogen. The red line depicts the evolution of gas irradiated by a strong UV background which corresponds to the direct collapse case (Figure 5a of Omukai, Schneider & Haiman 2008, [M/H] $= -6$) considered here. The red dashed line portrays the piecewise polytropic fit used in our simulations (see text). The blue line displays the evolution of metal-free gas in the absence of UV background (Omukai et al. 2005).

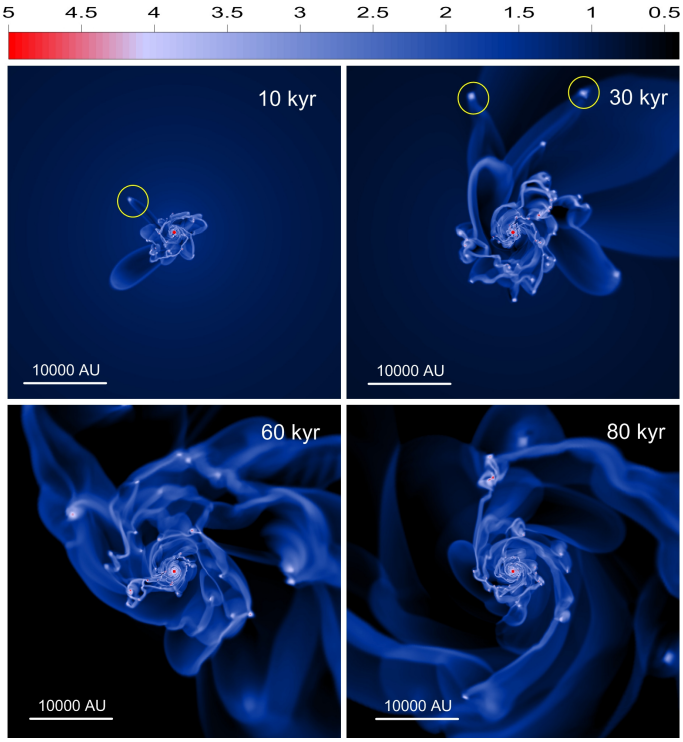

Figure 2. Images of the gas surface density in the inner 20000 $\times$ 20000 AU^2 box showing the evolution of the disc around the SMS star (represented schematically as a red circle in the coordinate center). The elapsed time since the formation of the star is indicated in each panel. Yellow circles indicate the fragments that are ejected from the disc. The scale bar is in g cm^{-2}.

We take this into account by parametrizing the fraction of accretion luminosity deposited onto the stellar surface,

$$\eta \equiv \frac{L_{*,\rm acc}}{L_{\rm acc}} = L_{*,\rm acc}\left(\frac{GM_*\dot{M}_*}{R_*}\right)^{-1}, \qquad (6)$$

where $L_{*,\rm acc}$ is the portion of accretion luminosity which contributes directly to the stellar luminosity and thus affects the stellar structure. As described in Hosokawa et al. (2013), the parameter η has a little effect on stellar evolution for high accretion rates $\gtrsim 0.1\ M_\odot\ {\rm yr}^{-1}$ aside from the earliest accretion phases. We assume $\eta = 0.1$ in our calculations.

The initial condition is a polytrope star of 2 $M_\odot$ with polytropic index $n = 1.5$, which well approximates a fully convective star. Before commencing with mass growth, the polytrope is allowed to first relax to a fully converged stellar model using STELLAR. The composition of the gas is assumed to be pristine with $X = 0.72$ and $Y = 0.28$. The accretion history is taken from the 2D hydrodynamical simulation (see Section 3.1).

3 RESULTS

3.1 Episodic mass accretion with self-gravitating discs

We start by describing the evolution of a circumstellar disc formed as a result of the gravitational collapse of our massive primordial core. Figure 2 presents the time evolution of the gas surface density in the inner 20000 $\times$ 20000 AU^2 box. The total computational region is about 10^2 times larger in area than shown in Figure 2. The elapsed time since the formation of the star (schematically shown by red circles in the coordinate center) is shown in each panel. Evidently, the disc is strongly gravitationally unstable and quickly breaks into giant spiral arcs. Gravitationally bound and pressure supported clumps form within these arcs via gravitational fragmentation.

In the absence of sink particles, tracking fragments during numerical simulations (on the fly) in grid-based codes becomes a challenging task. Therefore, we analyze the properties of the fragments in a post-process mode, using the method described in detail in Vorobyov, DeSouza & Basu (2013) in the context of discs around Population III stars. The algorithm is based on two conditions: The first one dictates that the fragment must be pressure supported, with a negative pressure gradient with respect to the center of the fragment. The second condition requires that the fragment be held together by gravity, with a positive gravitational potential gradient from the deepest potential well located at the center of the fragment.

The top panel in Figure 3 presents the number of fragments in the disc as a function of time. The number of fragments grows with time from a few tens immediately after the formation of the central star to more than a hundred by the end of our simulations. We note that the growth is not steady but is characterized by both increases and decreases in the number of fragments, implying that fragments can be both created and destroyed or otherwise lost by the disc. One such loss channel is accretion of the fragments onto the star caused by the loss of angular momentum due to gravitational interaction with other fragments and spiral arcs. This phenomenon is described in detail in Vorobyov & Basu (2006, 2010) in the context of present-day star formation

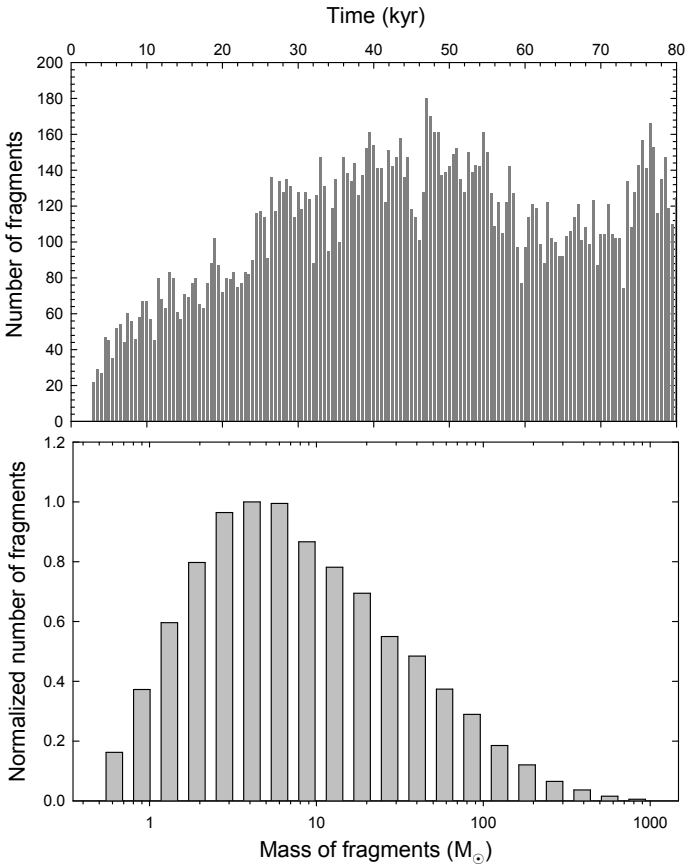

Figure 3. Top. Normalized number of fragments in the disc as a function of the elapsed time since the formation of the SMS star. **Bottom.** The distribution function of masses of the fragments formed in the disc at all times.

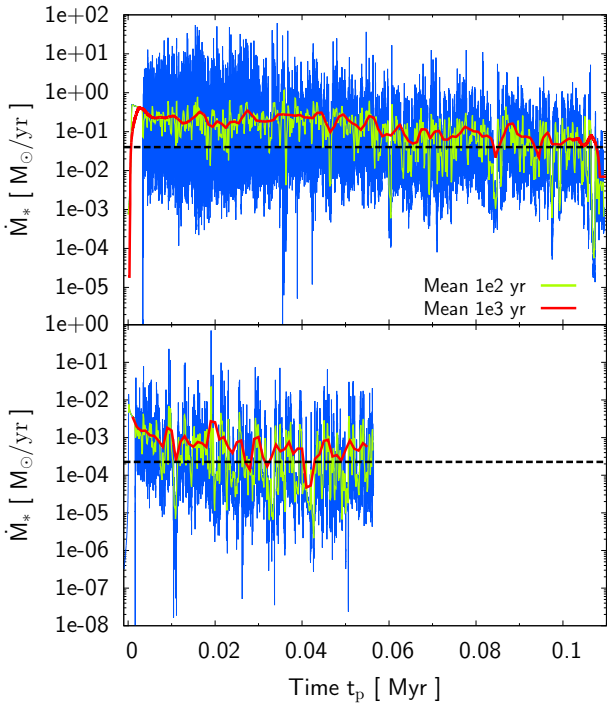

Figure 4. Comparisons of the accretion histories between the direct collapse and the normal Pop III cases. The origin of the time axis is the epoch of formation of the protostar. *Top panel:* the accretion history for the direct collapse case obtained by the 2D simulation. The blue line depicts the original accretion history without time averaging, and the red and green lines denote the time-averaged histories with bins of 10^3 and 100 years. *Bottom panel:* the accretion history for the normal Pop III case taken from Vorobyov, DeSouza & Basu (2013). The different colors have the same meanings as in the top panel. In each panel, the black dashed line indicates the threshold accretion rate below which the accretion is in the quiescent phase (see text).

and in Vorobyov, DeSouza & Basu (2013) in application to the formation of Pop III stars.

The number of fragments and the rate of their formation in our model disc is roughly a factor of 10 greater than was found in discs around present-day stars or normal Pop III stars (Vorobyov, Zakhozhay & Dunham 2013; Vorobyov & Basu 2015). This increase in the number of fragments is a consequence of the specific temperature vs. density relation typical for the direct collapse case. As the red line in Figure 1 demonstrates, there is a wide range of gas densities in the disc, $\leqslant 10^{16}$ cm^{-3}, for which the gas temperature decreases as the density increases. Any compression therefore creates a positive feedback for gravitational instability – an increase in density leads to a decrease in temperature, which in turn promotes further compression and, ultimately, fragmentation. An increased number of fragments leads to much higher accretion burst activity in SMS stars than for present-day or Pop III stars (see Figure 4 and Section 3.2 below).

The bottom panel in Figure 3 shows the normalized distribution function of masses of the fragments. We calculate the distribution function using all fragments identified in the top panel. Since the time sampling in the top panel is 500 yr, some long-lived fragments may be duplicated so that the calculated distribution function will be skewed towards long-lived fragments. The fragments vary in mass from a fraction of a solar mass to several hundred solar masses. Our simulations indicate that some of the fragments may be ejected out of the disc via multi-body interactions. Several such candidates are highlighted in Figure 2 by the yellow circles. If they can acquire sufficient velocities to escape the gravitational pull of the disc and the star, this may represent an interesting gateway for the formation of freely-floating primordial stars.

It is interesting to compare the variable accretion histories among the direct collapse case and the normal Pop III case studied by Vorobyov, DeSouza & Basu (2013), focusing on the duration of quiescent phases of the accretion $\Delta t_{\rm q}$. In order to quantify the duration of quiescent phases, we henceforth define the quiescent phases for the direct collapse case as phases when accretion rates are below 0.04 $M_{\odot}$ yr^{-1}, the critical rate above which the star enters the "supergiant" phase (see Section 1).

For the normal Pop III case, we define the quiescent phases as phases when the accretion rate falls below one tenth of the mean value. The definition is an analogy to that for the direct collapse case: the critical accretion rate below which accretion rates become quiescent is $\sim 0.1\times$ the mean accretion rate for the direct collapse case. In the following, we estimate $\Delta t_{\rm q}$ from the accretion histories for each case.

In Figure 4, the evolution of the accretion histories is shown for the direct collapse case (top panel) and the PopIII case (bottom panel). The accretion history is shown as a function of the elapsed time since the formation of a protostar $t_{\rm p}$. The blue line shows the original accretion history, while the red and green lines indicate the accretion histories averaged over $\Delta t_{\rm bin} = 10^3$ and 100 years, respectively. In each panel, the black dashed line is the threshold accretion rate $\dot{M}_{\rm th}$ below which the accretion is deemed quiescent. When averaging over $\Delta t_{\rm bin}$, all variations shorter than $\Delta t_{\rm bin}$ are smoothed. Thus, the duration of quiescent phases $\Delta t_{\rm q}$ will be less than $\Delta t_{\rm bin}$, if the accretion rate averaged over $\Delta t_{\rm bin}$ exceeds $\dot{M}_{\rm th}$. According to the above consideration, the typical duration of quiescent phases in the direct collapse case is much smaller than 10^3 yr for $t_{\rm p} \lesssim 0.06$ Myr, because the accretion rate averaged over 10^3 yr never falls below the threshold value and the accretion rate averaged over 10^2 yr seldom (and only for short periods of time $< 10^3$ yr) drops below the threshold value. The relatively long quiescent phases with $\Delta t_{\rm q} \sim 10^3$ years only appear in the late accretion stages for $t_{\rm p} \gtrsim 0.06$ Myr, because of the gradual depletion of the envelope mass with time and associated weakening of gravitational fragmentation in the disc. By contrast, the quiescent phases for the normal Pop III case are much longer, $\Delta t_{\rm q} \gtrsim 10^3$ years up to the end of the calculation, because the accretion rate averaged over both 10^2 yr and 10^3 yr falls below the threshold value for significant periods of time.

We attribute the above difference of $\Delta t_{\rm q}$ to the different intervals of disc fragmentation. As previously described, the disc in the direct collapse case is more unstable than in the normal Pop III case. This means that disc fragmentation is also more frequent. A greater rate of fragments infalling onto the star results in shorter durations of quiescent phases. The key quantity for the gravitational stability of the disc is the so-called Toomre Q parameter (Toomre 1964). It is known that, for the accretion stage of star formation, the Q parameter is approximately given by $Q \sim \mathcal{O}(0.1-1) \times (T_{\rm disc}/T_{\rm env})^{3/2}$, where $T_{\rm disc}$ and $T_{\rm env}$ are the temperatures of the disc and surrounding envelope (e.g., Kratter et al. 2010; Tanaka & Omukai 2014). For $T_{\rm disc} < T_{\rm env}$, the disc becomes more gravitationally unstable at a smaller Q value. As can be surmised from Figure 1, such a temperature imbalance can occur for the direct collapse case. In our 2D simulation, the number density at the boundary between the disc and envelope is $\sim 10^{6-9}$ cm^{-3} (see Figure 5). Since the temperature is a decreasing function of the density for $n_{\rm H} \lesssim 10^{16}$ cm^{-3}, the disc temperature is slightly lower than the envelope temperature. By contrast, the temperature imbalance between disc and envelope is opposite for the normal Pop III case, for which the temperature increases with increasing the density. This results in a less unstable disc, which explains the longer quiescent duration $\Delta t_{\rm q}$ seen in Figure 4.

Finally, in Figure 5 we present the azimuthally averaged gas surface and volume density as a function of distance from the star for two evolutionary times: one corresponding to the early evolution (10 kyr) and the other to the late evolution (60 kyr). Whereas low-mass fragments and spiral arcs are washed out by azimuthal averaging, the existence of massive fragments in the disc becomes apparent through the multiple short-wavelength peaks in the surface density distribution. The black circles mark the position of the disc outer edge.

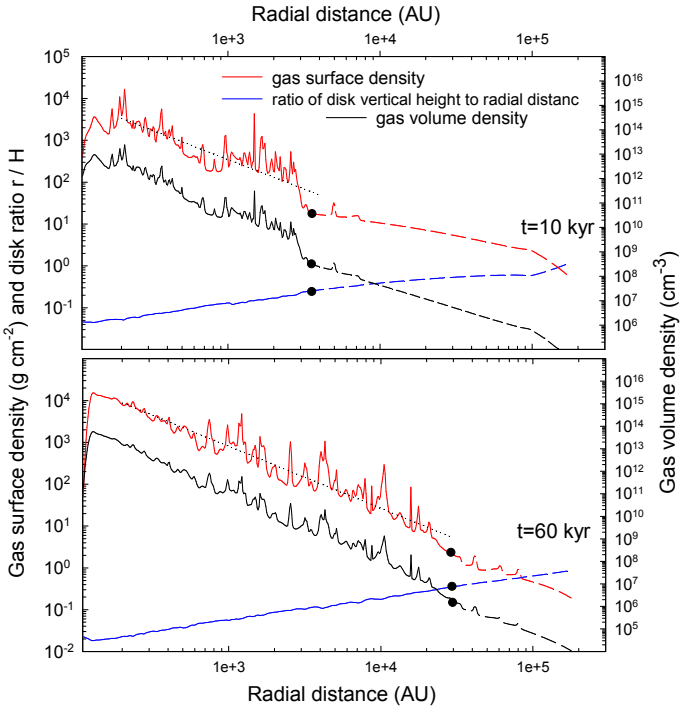

Figure 5. Azimuthally averaged gas surface and volume density profiles (red and black lines respectively) at two different evolutionary times after the formation of the star. The black circles mark the position of the disc outer edge. The black dotted lines provide the least-squares fits to the gas surface density profiles, which follow approximately an $r^{-1.5}$ law. The blue line is the ratio of the disc vertical scale height to the radial distance from the star. The outside regions of the disc are represented by the dashed lines.

The positions of the black circles is calculated visually taking into account that fragments (manifested by sharp local peaks in the density profiles) form within the disc, and not within the infalling parental core. The black circles therefore separate the regions with varying (disc) and smooth (core) density profiles. We note that applying more sophisticated disc tracking mechanisms (e.g., Dunham, Vorobyov & Arce 2014) has proven difficult for our highly unstable and fragmenting discs. Moreover, some fragments may be later scattered outside the disc owing to multi-body interactions, which would artificially increase our disc size estimates if we use the latter disc identification mechanism.

The black dotted lines are the least square fits to the surface density distribution in the disc. The corresponding relations at $t = 10$ kyr and $t = 60$ kyr are:

$$\Sigma\left[\frac{\rm g}{\rm cm^2}\right] = 10^{6.7\pm0.2}\left(\frac{r}{\rm AU}\right)^{-1.4\pm0.06}, \quad (7)$$

$$\Sigma\left[\frac{\rm g}{\rm cm^2}\right] = 10^{7.4\pm0.1}\left(\frac{r}{\rm AU}\right)^{-1.5\pm0.02}. \quad (8)$$

The disc surface density follows approximately an $r^{-1.5}$ law, also typical for self-gravitating discs around Pop III stars and in the local Universe (Vorobyov et al. 2013). The blue lines depict the ratio of disc vertical scale height to distance from the star. Evidently, this quantity stays well below unity everywhere in the disc, justifying the use of the thin-disc approximation.

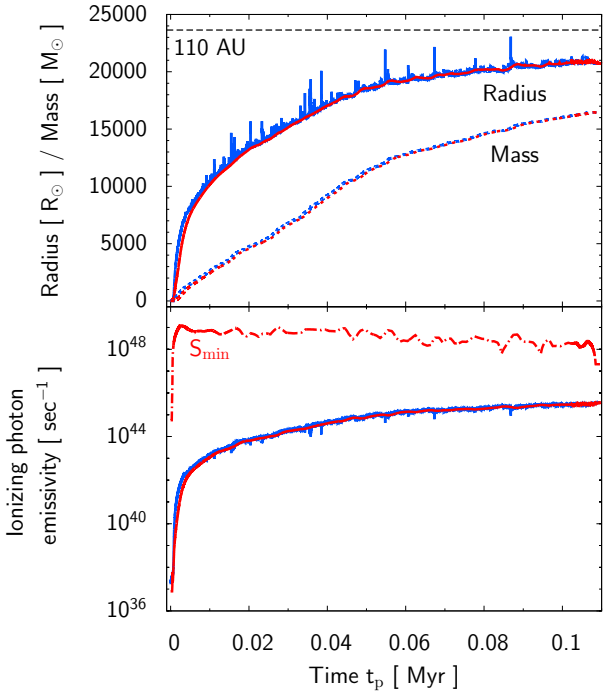

Figure 6. The time evolution of stellar mass and radius (top panel) and ionizing photon emissivity (bottom panel). The origin of the time axis is the epoch of formation of the protostar. The blue lines show the evolution without time averaging of the accretion rate (see Figure 4). The red lines show the evolution with the accretion rates averaged with time bins 10^3 yr. The black dashed line in the top panel indicates the sink radius of 110 AU. In the bottom panel, the dot-dashed line represents the critical value above which an HII region will appear (see Section 4).

3.2 Stellar evolution under episodic accretion

We now consider the evolution of the central protostar under the variable accretion history (blue curve in the top panel of Figure 4) obtained from the hydrodynamical simulation described in Section 3.1. Figure 6 shows the evolution of the stellar mass and radius and the ionizing photon emissivity. As seen in the top panel of Figure 4, the mean accretion rate approximately spans $\simeq 0.1 - 0.3\ M_\odot\ \mathrm{yr}^{-1}$, which is expected for the direct collapse model. Despite the frequent drops of the accretion rate below $0.04\ M_\odot\ \mathrm{yr}^{-1}$, which could in principle allow stellar contraction, the protostar's radius increases almost monotonically until the end of the calculation. The stellar radius reaches 100 AU at the end of the simulation, only slightly below the sink radius of 110 AU. This evolution is similar to that for constant accretion with rates of $\gtrsim 0.1\ M_\odot\ \mathrm{yr}^{-1}$ (e.g., Figure 1 of SHYY15). Not shown in the figure is the fact that the effective temperature remains almost constant at $\simeq 5000$ K due to the very sensitive temperature-dependence of H^- opacity. The ionizing photon emissivity therefore remains insufficient for creating an HII region.

SHYY15 concluded that, in order for the star to contract and leave the supergiant stage, the quiescent phase has to be longer than at least 10^3 years for $M_* \gtrsim 500\ M_\odot$. This explains the absence of contraction during the quiescent phases of our current simulations. SHYY15 derive the critical duration of 10^3 years at $500\ M_\odot$ by considering the typical KH timescale of supergiant protostars. As shown in previous studies (e.g., Hosokawa et al. 2013), the mass distribution in the interior of the bloated protostar is highly inhomogeneous; only a surface layer with a very small fraction of the total mass largely inflates to cover most of the stellar radius. SHYY15 have thus used the KH timescale only for the bloated surface layer $t_{\rm KH,surf}$ (see their equation 10), instead of the usual global definition $t_{\rm KH} \equiv GM_*^2/R_*L_*$. SHYY15 show that the surface KH timescale is approximately

$$t_{\rm KH,surf} \simeq 10 t_{\rm KH} \simeq 10^3\ \mathrm{yr} \left(\frac{M_*}{500\ M_\odot}\right)^{1/2}. \quad (9)$$

Since the quiescent phases found in our simulation are all shorter than this timescale, the inflated surface layer does not have enough time to contract by radiating away thermal energy. Even for the later stage $t_{\rm p} \gtrsim 0.06$ Myr when somewhat longer quiescent phases $\Delta t_{\rm q} \sim 10^3$ years appear, the star does not contract because $t_{\rm KH,surf}$ has also increased to $\gtrsim 10^3$ years with increasing stellar mass.

In order to evaluate the strength of UV feedback, we use the critical value of ionizing photon emissivity $S_{\rm min} = \dot{M}/\mu m_{\rm H}$: the value to ionize all of the atoms infalling onto the star once (see also SHYY15 and the discussion of HII region "squelching" by Yorke 1986). $S_{\rm min}$ is the lower limit to create an HII region in spherical geometry, because, in reality, additional UV photons are needed to ionize recombined atoms. Of course, the condition of "squelching" has to be fulfilled in all directions in order to entirely prevent an HII region from forming, and it is possible that a bipolar HII region could expand into the directions, from which little accretion occurs, but the extremely low UV flux ensures that the envelope can only be minimally affected by ionization. The bottom panel of Figure 6 also shows the evolution of $S_{\rm min}$, for which the accretion history averaged over 10^3 years is used. Since the UV emissivity for the current case is always much smaller than $S_{\rm min}$, no significant HII egion will appear to disturb the mass accretion.

4 CONCLUSION AND DISCUSSION

We have investigated the evolution of an accreting SMS and the resulting stellar UV emissivity resulting from realistic variable mass accretion rates generated by a self-gravitating circumstellar disc. The numerical hydrodynamics simulation gives evidence of very dynamic features of the disc and protostellar accretion; the disc readily fragments and the fragments then migrate inward to fall onto the star. The resulting accretion history is highly time-dependent, characterized by a number of short episodic accretion bursts followed by somewhat longer quiescent phases. Despite the strong variability of the accretion rate, the resulting stellar evolution is quite similar to that for constant accretion rates: namely, the stellar radius increases monotonically with increasing stellar mass. The effective temperature is almost constant at $\simeq 5000$ K, a temperature at which the star produces a negligible flux of UV photons. The absence of KH contraction during quiescent accretion phases is due to their short duration, $\Delta t_{\rm q} \lesssim 10^3$ years. As shown by SHYY15, this is shorter than the local KH timescale for the bloated stellar surface layer for $M_* \gtrsim 500\ M_\odot$. Since the surface layer can only inefficiently radiate away thermal energy in such a short time,

the star does not contract and leave the supergiant protostar stage.

In the current study, we have computed the evolution until the stellar mass reaches $\simeq 1.6 \times 10^4\ M_\odot$ (Fig. 6). As mentioned in Section 2.1, this is mostly due to our adopted initial conditions, in particular, the limited cloud mass of $\simeq 2.6 \times 10^4\ M_\odot$. It would be possible to simulate a longer evolution up to higher stellar masses assuming a higher initial cloud mass, but we focused on capturing the variability during the early stages of protostellar accretion, because the surface KH timescale is shorter for lower stellar masses $t_{\rm KH,surf} \sim 10^3$ yr $[M_*/10^3\ M_\odot]^{1/2}$.

We note that with the default sink size 110 AU, it is not until the stellar mass reaches $\simeq 1000\ M_\odot$ that the disc first appears. [1] A test case with a 70 AU sink shows that the disc and resulting accretion variability appear earlier for $M_* \gtrsim 700\ M_\odot$, for which $\Delta t_{\rm q}$ is still lower than 100 years as in the default case. Thus, we do not currently expect stellar contraction to occur in such early stages, a fact to be checked by future simulations. Note that we have not adopted the smaller sink, because the radius of the inflating SMS would soon exceed the sink size.

Although the top panel of Figure 4 shows that the duration of some quiescent phases becomes longer for $t_{\rm p} \gtrsim 0.06$ Myr, we expect that this is mostly due to the gradual depletion of the accretion envelope (Section 3.2). For more realistic cases of direct collapse, whereby significantly more massive clouds form in so-called atomic-cooling haloes, this mass depletion would be postponed to even later times. However, the duration of quiescent phases may increase for other reasons than envelope depletion. Following the discussion in SHYY15, the typical time lag between accretion bursts is proportional to the fragmentation timescale $t_{\rm frag} = M_{\rm d}/\dot{M}_{\rm d}$, where $M_{\rm d}$ is the disc mass and $\dot{M}_{\rm d}$ is the gas infall rate onto the disc (also see Vorobyov, Zakhozhay & Dunham 2013). From the fact that the disc mass increases in proportion to the stellar mass $M_{\rm d} \simeq 0.5\ M_*$ in our simulation, one may surmise that the fragmentation timescale also increases for $M_* \gtrsim 10^4\ M_\odot$. Since the typical duration of the quiescent phase is $\Delta t_{\rm q} \simeq 10^2$ years for $M_* \sim 10^4\ M_\odot$ (see top panel of Figure 4), $\Delta t_{\rm q}$ should reach $\sim 10^3$ years for $M_* \sim 10^5\ M_\odot$. Nevertheless, this is still ten times shorter than the surface KH timescale $t_{\rm KH,surf}$, which also increases with stellar mass. Therefore, we do not expect significant stellar contraction for higher SMS masses, until the stellar mass exceeds $\sim 10^5\ M_\odot$. At this point, the SMS is expected to collapse and produce a massive BH via the general relativistic instability.

5 ACKNOWLEDGEMENTS

YS thanks the support from Advanced Leading Graduate Course for Photon Science. EIV acknowledges the support from the Russian Ministry of Education and Science Grant 3.961.2014/K. This work was financially supported by Grant-in-Aid for JSPS Fellows (15H00776: YS), by JSPS-OEAD short-term research grant #RC (21402003: EIV), and by the Grants-in-Aid for Basic Research by the Ministry of Education, Science and Culture of Japan (25800102, 15H00776: TH, 25287040: KO, 25287050: NY). Portions of this work were conducted at the Jet Propulsion Laboratory, California Institute of Technology, operating under a contract with the National Aeronautics and Space Administration (NASA). Numerical simulations were done on the Vienna Scientific Cluster (VSC-2), Atlantic Computational Excellence Network (ACEnet), and Shared Hierarchical Academic Research Computing Network (SHARCNET). The stellar evolution calculations were partly conducted on a PC cluster at the Center for Computational Astrophysics, National Astronomical Observatory of Japan.

[1] The smaller the sink cell, the earlier the disc forms – disc formation occurs when the infalling material first hits its centrifugal barrier. With our chosen initial conditions, the lower angular momentum material, which hits its centrifugal barrier closer to the central star, arrives earlier.

REFERENCES

Agarwal B., Smith B., Glover S., Natarajan P., Khochfar S., 2015, ArXiv e-prints
Basu S., 1997, ApJ, 485, 240
Becerra F., Greif T. H., Springel V., Hernquist L. E., 2015, MNRAS, 446, 2380
Bromm V., Loeb A., 2003, ApJ, 596, 34
Colella P., Woodward P. R., 1984, Journal of Computational Physics, 54, 174
Dunham M. M., Vorobyov E. I., Arce H. G., 2014, MNRAS, 444, 887
Fan X., Strauss M. A., Richards G. T., Hennawi J. F., Becker R. H., White R. L., Diamond-Stanic A. M., 2006, AJ, 131, 1203
Fan X., Strauss M. A., Schneider D. P., Becker R. H., White R. L., Haiman Z., Gregg M., Pentericci L., 2003, AJ, 125, 1649
Fernandez R., Bryan G. L., Haiman Z., Li M., 2014, MNRAS, 439, 3798
Greif T. H., Bromm V., Clark P. C., Glover S. C. O., Smith R. J., Klessen R. S., Yoshida N., Springel V., 2012, MNRAS, 424, 399
Hosokawa T., Hirano S., Kuiper R., Yorke H. W., Omukai K., Yoshida N., 2015, ArXiv e-prints
Hosokawa T., Omukai K., Yoshida N., Yorke H. W., 2011, Science, 334, 1250
Hosokawa T., Yorke H. W., Inayoshi K., Omukai K., Yoshida N., 2013, ApJ, 778, 178
Inayoshi K., Omukai K., 2012, MNRAS, 422, 2539
Inayoshi K., Visbal E., Kashiyama K., 2015, ArXiv e-prints
Kratter K. M., Matzner C. D., Krumholz M. R., Klein R. I., 2010, ApJ, 708, 1585
Latif M. A., Volonteri M., 2015, MNRAS, 452, 1026
Machida M. N., Inutsuka S.-i., Matsumoto T., 2010, ApJ, 724, 1006
McKee C. F., Tan J. C., 2008, ApJ, 681, 771
Mortlock D. J. et al., 2011, Nature, 474, 616
Omukai K., Schneider R., Haiman Z., 2008, ApJ, 686, 801
Omukai K., Tsuribe T., Schneider R., Ferrara A., 2005, ApJ, 626, 627
Regan J. A., Johansson P. H., Haehnelt M. G., 2014, MNRAS, 439, 1160
Sakurai Y., Hosokawa T., Yoshida N., Yorke H. W., 2015, MNRAS, 452, 755

Schleicher D. R. G., Palla F., Ferrara A., Galli D., Latif M., 2013, A&A, 558, A59
Smith R. J., Hosokawa T., Omukai K., Glover S. C. O., Klessen R. S., 2012, MNRAS, 424, 457
Stone J. M., Norman M. L., 1992, ApJS, 80, 753
Sugimura K., Omukai K., Inoue A. K., 2014, MNRAS, 445, 544
Tanaka K. E. I., Omukai K., 2014, MNRAS, 439, 1884
Toomre A., 1964, ApJ, 139, 1217
Truelove J. K., Klein R. I., McKee C. F., Holliman, II J. H., Howell L. H., Greenough J. A., 1997, ApJ, 489, L179
Vorobyov E. I., 2013, A&A, 552, A129
Vorobyov E. I., Basu S., 2006, ApJ, 650, 956
Vorobyov E. I., Basu S., 2009, MNRAS, 393, 822
Vorobyov E. I., Basu S., 2010, ApJ, 719, 1896
Vorobyov E. I., Basu S., 2015, ApJ, 805, 115
Vorobyov E. I., DeSouza A. L., Basu S., 2013, ApJ, 768, 131
Vorobyov E. I., Zakhozhay O. V., Dunham M. M., 2013, MNRAS, 433, 3256
Willot M., Christmann M., 2010, Nature Chemistry, 2, 519
Wu X.-B. et al., 2015, Nature, 518, 512
Yorke H. W., 1986, ARA&A, 24, 49
Yorke H. W., Bodenheimer P., 2008, in Astronomical Society of the Pacific Conference Series, Vol. 387, Massive Star Formation: Observations Confront Theory, Beuther H., Linz H., Henning T., eds., p. 189